Applied Physics A (2022) 128:342
https://doi.org/10.1007/s00339-022-05464-6

Applied Physics A
Materials Science & Processing

Magnetic properties of exchange-biased FeCo/CoO bilayer and its electronic structure

Ratnesh Gupta[1] · K. Sangeeth[1] · M. Gupta[2] · R. J. Choudhary[2] · A. Sagdeo[3] · F. Singh[4] · Ajay Gupta[5]

Received: 4 September 2021 / Accepted: 4 March 2022 / Published online: 25 March 2022

Abstract

Magnetic and structural properties of FeCo/CoO bilayer prepared by ion beam sputtering on silicon substrate have been studied. As-deposited specimen exhibits exchange bias at 10 K. The influence of thermal annealing and swift heavy ion on the exchange bias field has been studied. Thermal annealing enhances the value of exchange bias field (H_{EB}) as well as magnetic moment of the bilayer; revealing that the exchange bias value is tailored by the thermal annealing and depends upon annealing temperature. X-ray diffraction gives convincing support of the phase formation of Co_3O_4 in the CoO layer after thermal annealing. A correlation has been observed between soft X-ray absorption and the corresponding magnetic characteristics. The exchange bias effect exists up to temperatures beyond the ordering temperature of the Cobalt oxide layer. Upto the 6×10^{13} ions/cm^{2}of 100 MeV Au-ion irradiation does not change the magnetization behaviour of the FeCo/CoO system. Higher ion fluence of 1×10^{14} Au-ions/cm^2, reduces the H_{EB}value. Thermal annealing enhances the H_{EB} value. From the soft X-ray absorption, it reveals that the reduction in the H_{EB} value for the ion-irradiated specimen is due to defects present in the film.

Keywords Iron–Cobalt Thin Film · Phase transition · Exchange bias · Ion beam irradiation · Swift heavy ion · Anti-ferromagnet

1 Introduction

The exchange bias (EB) effect is a well-known and extensively studied phenomenon existing in artificially prepared thin films at the interface of a ferromagnet (FM) and an anti-ferromagnet (AFM) material providing a unidirectional magnetic anisotropy [1, 2]. Exchange bias effects have been rigorously studied in several systems in the form of thin FM/AFM bilayers and core–shell clusters [2]. However, regardless of the several theoretical and experimental studies [3–8], the behavior of exchange anisotropy is not yet fully understood at the microscopic level. From the application point of view, thin film structures which generally possess FM coupled with an AFM are the most useful and relevant. For example, exchange bias thin film structures are the part of spin-valve devices, based on giant magneto-resistance effect [9, 10]. Technologically, the concept of unidirectional exchange anisotropy can be extensively used in magnetic random access memory (MRAM) [11, 12] and in required directions in hard disk drive read/write heads [13–15] for pinning FM layers. Up to now, lot of experimental investigations in the field of exchange bias have been mostly focused on the studies of artificially prepared systems, for example: core–shell nano-particles with the FM core coupled to the AFM shell [16, 17], bi-layer or multilayer films consist of FM and AFM thin layers [18], or bi-layer systems like Fe/FeF_2, where a spin glass like behavior has been used to understand the EB effect [19]. It has been observed that the exchange bias exists not only in artificially prepared systems, but also in cobaltite [20] and bulk perovskite manganite [21, 22]. The phenomena of EB is a complicated magnetic

✉ Ratnesh Gupta
gratnesh_ioi@yahoo.com

1 School of Instrumentation, Devi Ahilya Vishwavidyalaya, Khandwa Road, Indore, India

2 UGC-DAE CSR, Indore Centre, Khandwa Road, Indore, India

3 Indus Synchrotron Utilization Division, Raja Ramanna Center for Advanced Technology, Indore 452013, India

4 Inter-UniversityAccelerator Centre, New Delhi, India

5 Physics Department, University of Petroleum and Energy Studies, Dehradun, India

interaction, which occurred at the vicinity of FM and AFM layers, and it depends on spin geometries, coupling strength of the materials, and also upon different magnetization reversal processes.

In the present work, we have study the effects of swift heavy ion irradiation and thermal annealing on FeCo/CoO bilayer and correlate the magnetic properties with its electronic structure. The magnetic moment of FeCo is highest among the 3d-ferromagnet as well as it is a soft magnetic material [23]. The magnetostriction constant of the FeCo is quite high, therefore even a small modification in the structure changes the magnetic properties significantly [24]. The FeCo material is highly oxidation resistant, therefore perturbation from the oxide layer is minimal and hence it can be a probable material for the magnetic devices. CoO is a well-known AFM material, systems like Fe/CoO, Co/CoO are well studied to understand the different aspects related to exchange bias phenomenon [25, 26]. Different phases of Co-oxides either behaves as anti-ferromagnetic material or as ferrites [27, 28]. In both the cases, a modification in Co-oxides does not obstruct the exchange bias behavior. Thus, modification by ion-irradiation or annealing will modify the exchange bias behavior.

2 Experimental procedure

FeCo/CoO/Si(100) hetero structure was deposited by ion beam sputtering method where cobalt oxide was grown in the presence of 5:3 Argon to Oxygen ratio at room temperature. The base pressure and the working pressure were maintained at 2×10^{-8} mbar, and 2×10^{-5} mbar, respectively. The aluminium 2.0 nm has been capped on top of it. Figure 1 shows the schematic picture of the specimen. The vacuum annealing (2×10^{-6} mbar) of the specimens has been performed for 1 h at 573 K and 673 K. The time taken to achieve annealing temperature of 573 K and 673 K from room temperature is 20 min. and 30 min., respectively. The fabricated sample was subjected to 100 MeV $Au8^{+}$ ion irradiation with different ion fluence ranging from 1×10^{12} ions/cm^2 to 1×10^{14} ions/cm^2. For irradiation, we have used Pelletron accelerator at IUAC, New Delhi, India. The structural studies of the film were performed using Angle Dispersive X-Ray Diffraction (ADXRD) ($\lambda=0.7356$ Å (17 keV)) on BL-12 of INDUS II Synchrotron Radiation Centre, Indore India. The soft X-ray absorption spectroscopy (SXAS) measurements on thin film samples were done on BL-1 beam-line of INDUS-II. Room temperature spectrum of Fe $L_{3,2}$, Co $L_{3,2}$ and O K-edge, edges were measured in total-electron-yield (TEY) mode. Total magnetization of the film was performed at 10 K in field cooled (FC) mode in 1.5 kOe applied magnetic field using Quantum design SQUID-VSM. The temperature-dependent Zero field cooled (ZFC) and field cooled (FC) magnetization curves were measured upon heating from 10 to 300 K.

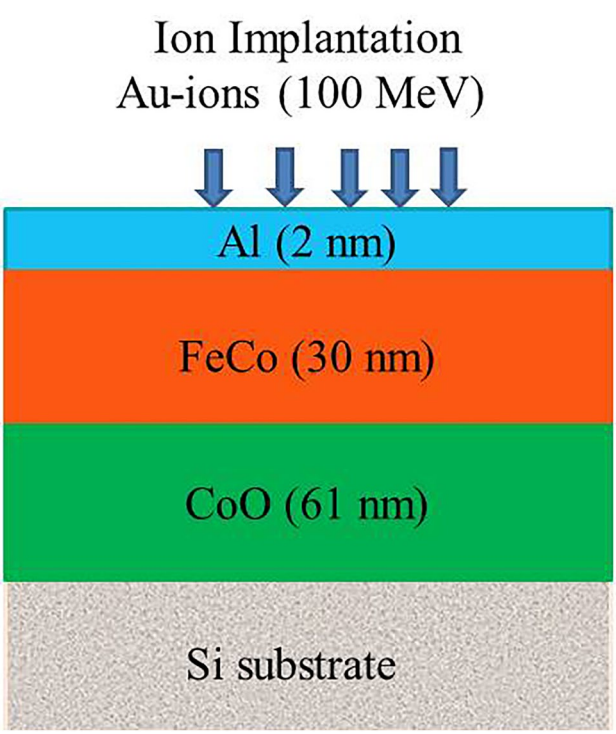

Fig. 1 Schematic picture of the exchange bias thin film on Si substrate

3 Result and discussion

The ADXRD scans of as-deposited, irradiated samples (with various ion fluences) and after annealing at different temperatures have been given in Fig. 2. The as-deposited sample is found to be composed of the bcc FeCo phase and the mixed cobalt oxide phases such as CoO, Co_3O_4. In the as-deposited specimen, and a very broad peak has been observed for the mixed disordered cobalt oxide phases. After the Au-ion irradiation, the FeCo peak in the corresponding ADXRD data is slightly shifted towards left side and the lattice constant of the FeCo [110] is reduced with increasing ion-fluence. Its lattice constant value has been changed from 2.836 Å to 2.832 Å after the ion fluence of 1×10^{14} ions/cm^2. Gupta et.al. have studied the effects of swift heavy ions on FeCo thin film and observed that the main peak of FeCo(110) have been shifted towards left as a function of ion-fluence [24]. The lattice constant of CoO after ion-fluence of 6×10^{13} ions/cm^{2}becomes 4.841 Å from 4.915 Å. Perusal of Fig. 2 shows that the annealing of the as-deposited samples at 573 K and 673 K for 1 h. After the annealing at 673 K, the individual FeCo peak has been shifted towards left and the peak position has been changed from 3.1326 Å^{-1} to 3.1292 Å^{-1}. For

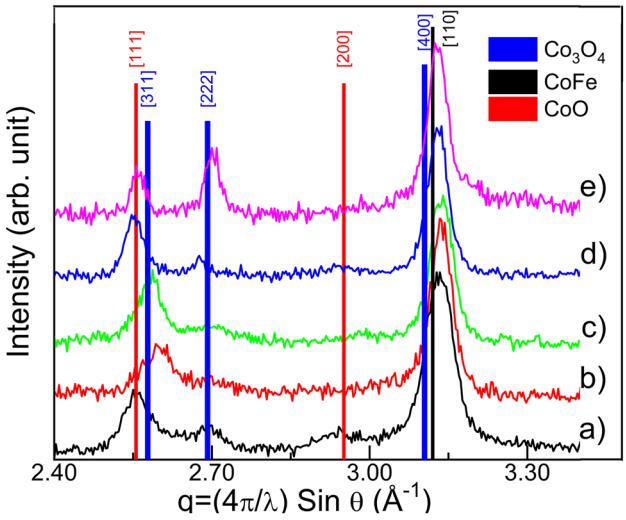

Fig. 2 Angle dispersive X-ray diffraction pattern of **a** as-deposited, **b** ion fluence 6×10^{13} ions/cm^2, **c** ion-irradiated with ion fluence 1×10^{14} ions/cm^2, **d** annealing at 573 K and **e** annealing at 673 K

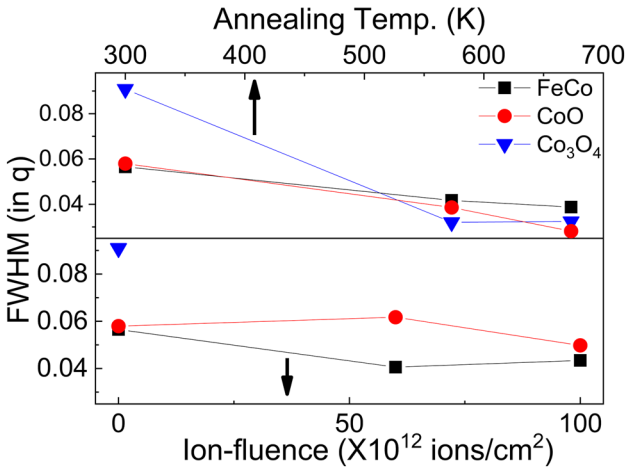

Fig. 3 Full width at half maximum for main peak of CoO, FeCo for **a** as-deposited and ion-irradiated specimens, **b** after thermal annealing

the FeCo(110) BCC lattice, the lattice constant has been calculated by simply [$2\pi\times\sqrt{2}/q$], therefore the lattice constant of FeCo after annealing becomes higher and it increases with annealing temperature. It changes from 2.837 Å of the as-deposited specimen to 2.840 Å after the annealing at 673 K. Figure 2 clearly shows that the peak at $q=2.68$ Å^{-1} emerge very sharply compared with the specimen annealed at 573 K, this particular peak clearly suggest the formation of Co_3O_4 phase. The peak intensity of Co_3O_4 phase has been increased after the annealing of new sample from 300 to 673 K, it clearly reveals the phase transformation has been occurred from CoO to Co_3O_4 because of annealing. This phase transformation generally occurs, when the specimen has been annealed at 633 K or more [29]. It occurs due to the following solid state reaction [30, 31]:

$$4CoO \rightarrow Co + Co_3O_4. \quad (1)$$

Langell et al. have also observed the phase transformation of epitaxial CoO into Co_3O_4, when they anneal the specimen at 623 K at 1.33×10^{-4} mbar oxygen pressure for 30 min or more [29]. In our case, the pressure in the chamber during annealing was 2×10^{-6} mbar. Figure 3a shows the FWHM of the main peaks of different components available in the specimen before and after ion-implantation. The FWHM of the peaks is reduced after ion irradiation, which suggests that the stresses present in the film during deposition has been relieved by ion irradiation. After annealing the FWHM of the peak correspond to CoO, Co_3O_4, and FeCo are reduced drastically (shown in Fig. 3b). The reduction in the lattice constant of the film after the irradiation can be easily explained using the concept of energy deposition mechanism during the irradiation process. The high electronic excitations are responsible for the modification in the FeCo/CoO structure [32–35]. The electronic energy loss has been dependent possibly on the energy transfer process between the energetic irradiated ion species (Au-ions) and the target atoms (FeCo/CoO thin film). It can be easily understand using thermal spike model [36, 37]. In the thermal-spike model, the maximum energy of the bombarded ions is transferred to the target electrons during electronic slowing-down regime. It causes to increase the temperature of the electronic subsystem, beyond its melting temperature. However, this fast heating is confined near to the travel-path of the ion in the material, followed by a rapid quenching in the order of 10^{13}–10^{14} K/s. Thus, when the swift heavy ion passes through the FeCo/CoO, the rapid thermal quenching process have been occurred after the massive heating may causes higher energetic configuration and as a consequence decrease in the volume of unit-cell. Beyond threshold value, further increment in the ion-fluence may enhance a fast increase in energy density, and also the mean free path between displacing collisions advances the inter-atomic spacing of the material [38, 39]. At this stage, the succeeding thermal quenching may lead to the disordered state. It is due to 100 MeV Au ions, which corresponds to electronic energy loss for FeCo and CoO of 31.39 keV/nm and 21.93 keV/nm, respectively, as calculated by SRIM software [40].

To study the impact of ion-irradiation and the thermal annealing, magnetic properties of FeCo/CoO have been studied at 10 K. Figure 4 shows magnetization hysteresis loops (performed at 10 K after cooling from room temperature in presence of an applied field of 1.5 kOe) measured for as-deposited, ion-irradiated and after annealing at different temperatures. The definition of the exchange bias

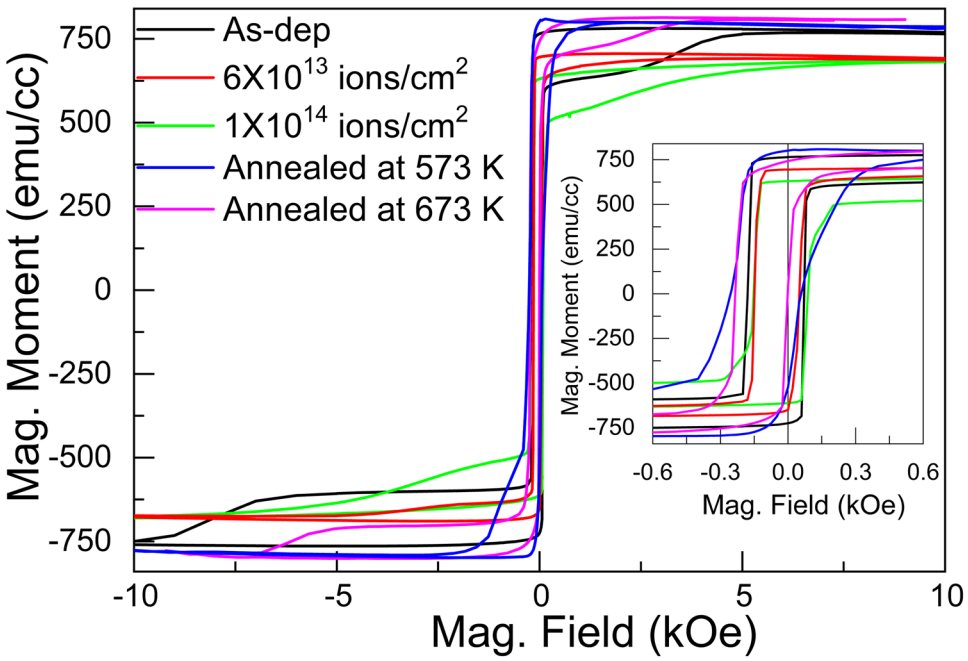

Fig. 4 Magnetization curve at 10 K under field cooled condition (1.5 kOe) for as-deposited and treated specimens

Table 1 Magnetic moment, coercivity and exchange bias field value obtained from magnetization curves

Sample details	Coercivity (Oe)	H_{EB} value (Oe)	Magnetic moment (emu/cc)
As-deposited	125.2	55.6	765.9
6×10^{13} Au-ions/cm^2	99.85	49.4	678.5
1×10^{14} Au-ions/cm^2	119.1	31.9	676.9
Annealing at 573 K	154.7	101.6	784.4
Annealing at 673 K	116.0	115.3	799.7

field value $H_E=(H_{C2}+H_{C1})/2$ and the coercivity of the film is $H_C=(H_{C2}-H_{C1})/2$, where H_{C1} and H_{C2} are the coercive fields on the left and right side of the hysteresis loop, respectively. The magnetization curve of as-deposited specimen is shifted towards negative field. The magnetic moment of the as-deposited film is 765.90 emu/cc and it exhibits exchange bias at 10 K after field cooled the specimen from room temperature to 10 K. The magnetic moment of the film, given in Table 1 is reduced after ion irradiation and its exchange bias value has also been decreasing. It may be due to surface roughness occurred because of sputtering during the ion-irradiation as well as the interface between FeCo/CoO becomes rough which reduces the exchange bias in the field. After annealing, the magnetic moment of the bilayer film have been increasing slightly. It may be due to phase transformation from CoO to Co_3O_4 as evidenced by corresponding XRD patterns and the formation of ferrites at the interface which increases the magnetic moment of the film. Regan et.al. have studied the chemical and magnetic studies of FM/AFM Oxides [41]. They observed that at the FM/AFM interface, 2–3 monolayers of the Metal/oxides close to interface have been oxidized/reduced. The exchange bias value after annealing at 673 K has been increased from 55.6 Oe to 115.33 Oe. This result reveals that the hetero-structure formation of CoO, Co_3O_4 and ferrites at the interface contributes to increase in the exchange bias. Vaz et al. have shown that in case of Ni/Co_3O_4 specimen the exchange bias value has been increased after annealing. They suggested that the surface morphology of Co_3O_4 has a significant influence on the exchange anisotropy [42]. It has been further supported by the fact that the annealing reduces the defects and stress present in the film which supports the saturation of the magnetization to decrease the coercivity of the film, as given in Table 1.

Apart from the magnetic hysteresis curves, the temperature dependence of the magnetization after Zero field cooling (ZFC) and field cooling (FC) is useful to know the influence of ion-irradiation and thermal annealing. Figure 5 represents the ZFC and FC magnetization curves of as-deposited thin film and for the films after the ion fluence of 1×10^{14} Au-ions/cm^2 and after the annealing at 673 K. Perusal of Fig. 5 showed that the ZFC and FC magnetization curves gives different irreversibility features in differently treated specimens. In the as-deposited specimen, the ZFC curve displays a sharp increase at about $T_B\approx225$ K. When both the ZFC and FC curves are bifurcated, this specific

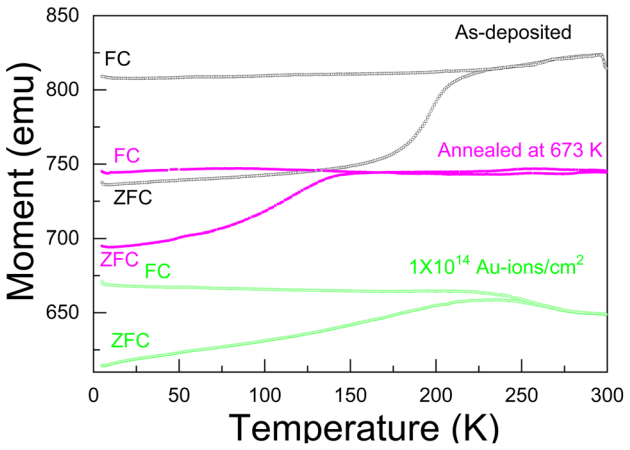

Fig. 5 Zero field cooled (ZFC) and field cooled (FC) magnetization curves measured in an applied field of 1.5 kOe for an as-deposited, ion irradiated with the Au-fluence of 1×10^{14} ions/cm^2 and annealed sample at 673 K

temperature is defined as blocking temperature. For the 1×10^{14} ions/cm^2 Au-ion irradiated specimen and thermally annealed specimen at 673 K shows the blocking temperature at 250 K and 145 K, respectively. The deviation of the ZFC and FC curves clearly suggest that a fraction of total moment is frozen and it cannot be reversed back in a high external field demonstrate that a strong exchange coupling between FM/AFM is present at the interface. The Neel temperature of Co_3O_4 and CoO is lower than 40 K and 290 K, the loop shifts continued up to ~ 250 K or above, indicating the existence of the exchange coupling between FeCo and Co-Oxides [43, 44]. However, existence of EB above Neel temperature was also reported in Co/FeF_2 [45] and it is due to short range magnetic ordering above Neel temperature. In case of $Fe_{0.6}Zn_{0.4}F_2$ (110)/Fe(14 nm)/Ag(35 nm) heterostructures, the improvement of the blocking temperature has been observed [46], it was due to the presence of Griffiths phase–like finite clusters. Increment in the coercivity was also reported in layered Fe/FeF_2 above Neel temperature, because of spin fluctuations in the antiferromagnetic FeF_2 [47].

To understand the increase in magnetic moment of FeCo/CoO bilayer after annealing, we have performed SXAS measurements. This measurement technique is suitable for the chemical environment as well as it is element specific, to investigate the interface of a FM metal and AFM oxides. The Fe L edge spectra consist of L_3 and L_2 corresponding to the respective 2p3/2 and 2p1/2 characters of the core hole, split by the 2p spin–orbit coupling. Figure 6a shows the Fe 2p X-ray absorption spectra of as-deposited, ion-irradiated and after annealing samples. Perusal of as-deposited spectrum in Fig. 6a clearly shows that the L3 peak consist of two peaks at about 708 eV and 709.5 eV. The peak at 708 eV corresponds to bcc Fe and at 709.5 eV may be attributed to possible oxide. The L-edge Fe spectrum and its different oxides have been studied in detail [41, 48–51]. After the treatment, the intensity of the peak at 708 eV has been reduced clearly suggest that some oxides have been formed during annealing as well as during ion-beam irradiation. From the Fig. 6a, one may note that there is no significant changes have been observed after different kind of treatments. It clearly suggest that the composition of iron oxide and its amount has been the same for all the four treated specimens. In the lower panel of Fig. 6a, we plotted the simulated data using CTM4XAS code [52] for pure Fe as Fe^{2+} with + 1.0 eV as10 Dq value and Fe + 3 with two different values of 10 Dq. Because the L3 spectrum of Fe_3O_4 contains a main peak which correspond to Fe^{3+} ions at both octahedral (10Dq = − 0.6 eV) + tetrahedral sites (10Dq = + 1.6 eV) and a shoulder at lower energy due to Fe^{2+} ions which is about 1.4 eV below the main peak [49]. There is no change in the composition of Iron oxide after ion-irradiation as well as thermal annealing, thus the contribution in enhancement in the magnetic moment of the film as well as the increment in the HEB value is due to the formation of different phases of Cobalt oxides.

The Co L-edge spectra consists of L_3 and L_2 corresponding to the respective 2p3/2 and 2p1/2 characters of the core hole, split by the 2p spin–orbit coupling. In Fig. 6b, the Co 2p X-ray absorption spectra of as-deposited, ion-irradiated and after annealing samples are presented. As-deposited specimen shows the broad L_3 and L_2 peak, which may correspond to CoO. As-deposited specimen shows the broad L_3 and L_2 peak, which may correspond to CoO. There are no significant changes in the ion-irradiated spectra. In case of annealed specimen, the spectra become more broadened (towards right side) and a peak at about 780 eV has been observed after the annealing at 673 K. Inset shows the clear evolution of this peak after annealing. Bazin et al. have studied the Co X-ray absorption spectra of CoO and Co_3O_4 [53]. In case of CoO, they observed a fine structure at L_3 edge and for Co_3O_4 (as evidenced by the corresponding ADXRD patterns), a shifted main peak at about 779 eV has been observed, corresponds to Co^3. In the lower panel of Fig. 6b, one can see the charge transfer multiplet calculations for Co^{2+} (tetra) and Co^{3+} (octahedral) and compared with the experimental XAS data [41]. Perusal of Fig. 6b, clearly suggest that the qualitatively Co^{3+} site has been formed after the annealing of FeCo/CoO bilayer. Co_3O_4 possess normal spinel structure with non-magnetic Co^{3+} ions located at octahedral site while magnetic Co^{2+} ions are situated at tetrahedral site. The overall magnetization of this compound is due to presence of extended super-exchange pathway of Co^{2+}–O–Co^{3+}–O–Co^{2+} situated at intermediate site between O^{2-} ions [43, 54]. Recently, AFM CoO–Co_3O_4 octahedragives a ferromagnetic behavior at room temperature [55].

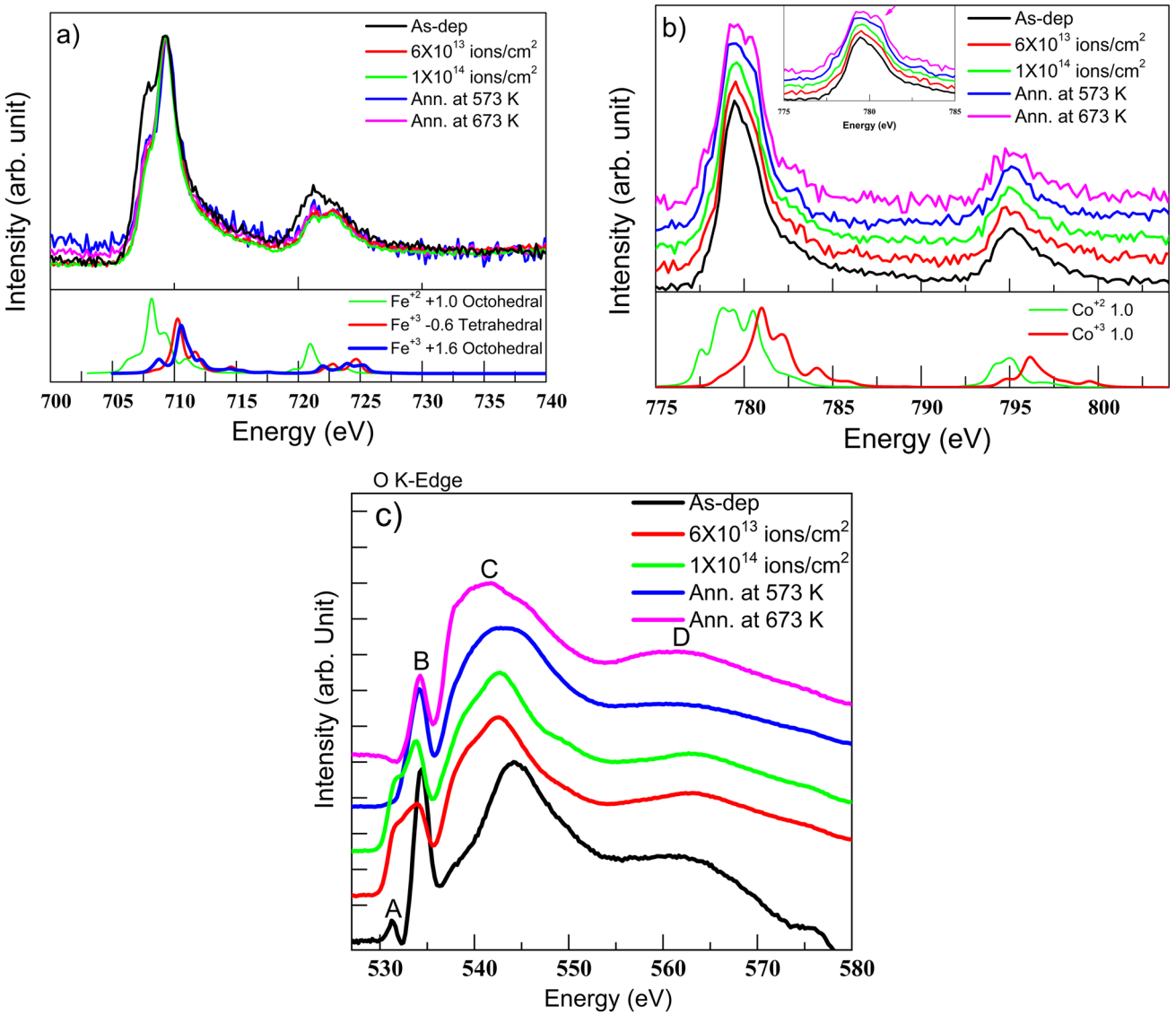

Fig. 6 **a** Normalized Fe L3,2 edge, XAS spectra of as-deposited and treated specimens. Lower panel of fig. shows the simulated data using CTM4XAS code [52] for pure Fe as Fe^{2+} with + 1.0 eV as10 Dq value and Fe^{3+} with two different values of 10 Dq. **b** Normalized Co L3,2 edge XAS spectra of as-deposited and treated specimens. Inset shows the 2p3/2 peak positions. Lower panel of fig. shows the simulated data using CTM4XAS code [52] for Co^{2+} (tetra) and Co^{3+} (octahedral) with different values of 10Dq values. **c** Normalized O k-edge XAS spectra of as-deposited and treated specimens

Further the annealing of CoO in between 573 and 673 K possesses ferromagnetic behavior at room temperature. Thus, in our present case, the higher value of magnetic moment compared to as-deposited is due to the formation of super-exchange pathway. The O K-edge XAS spectra before and after treatments are shown in Fig. 6c. The spectrum gives transitions of oxygen p character hybridized with cobalt 3d states and above 533 eV to oxygen p character in the cobalt 4sp band [56]. It showed many features, namely the peak A at 531 eV, peak B at 534 eV and the broad feature C and D extending in the range 535–550 eV and 550–580 eV. The XAS spectra at the O K-edge exhibit evident changes of the intensity of the peak A with ion-irradiation and after thermal annealing. The intensity of peak A is increasing after the ion-irradiation, while it is completely vanished in case of annealing and the peak B becomes stronger. It clearly suggests that the hybridization between Fe, Co and O is different for the ion-irradiated specimens and annealed specimens. From the Fig. 6c, it clearly reveal that the features at the O-edge arises due to covalent mixing of the metal and oxygen states, which presents oxygen p character in unoccupied states of mainly metal character. The as-deposited and irradiated spectra can be divided into two regions: (i) it is a double-peak sharp structure near 530 eV, which

can be related to the metal 3d states and defect states; (ii) Beyond 535 eV is because of O2p and O3p transitions with the higher lying bands of different metals. Ion-irradiation enhances the defect states in the specimens, which enhances the intensity of the peak near to absorption edge after the ion-fluence of 6×10^{13} ions/cm^2 and it becomes higher with the ion fluence of 1×10^{14} ions/cm^2. After thermal annealing, the double peak structure becomes single peak structure and we argue that the defects present in the as-deposited specimens are reduced upto a large extent. It can also be evidenced by the reduction of coercivity after annealing due to reduction in the defect density in the film.

4 Conclusion

The FeCo/Co-oxide films have been prepared by ion beam sputtering and it exhibits the exchange bias below the Neel temperature of CoO. Ion irradiation upto 6×10^{13} Au ions/cm^2, does not significantly change the magnetization behavior at 10 K. At the ion-fluence of 1×10^{14} Au ions/cm^2, the value of H_{EB} decreases and the magnetic moment also decreases. Annealing of FeCo/CoO films induces a phase transformation from CoO into Co_3O_4, which enhances the exchange bias field in the film. It has been also clearly evidenced in the corresponding soft X-ray absorption spectrum. Higher magnetic moment of the film after annealing is due to charge transfer process. Temperature-dependent magnetization behavior in case of FC and ZFC is also different in all the three cases. Different hybridization has been observed for the ion-irradiated specimen as well as thermally annealed specimen. Higher magnetic moment of the film after thermal annealing may be due to super-exchange pathways.

Acknowledgements This work has been funded by UGC DAE CSR Indore and IUAC, New Delhi.

Data availability The data that support the findings of this study are available from the corresponding author upon request.

Declarations

Conflict of interest There is no financial interests.

References

1. J. Nogués, I.K. Schuller, J. Magn. Magn. Mater. **192**, 203 (1999)
2. A.E. Berkowitz, K. Takano, J. Magn. Magn. Mater. **200**, 552 (1999)
3. J. Nogues, J. Sort, V. Langlais, V. Skumryev, S. Surinach, J.S. Munoz, M.D. Baro, Phy. Rep. **422**, 65 (2005)
4. K. O'Grady, L.E. Fernandez-Outon, G. Vallejo-Fernandez, J. Magn. Magn. Mater. **322**, 883 (2010)
5. R.L. Stamps, J. Phys. D **33**, R247 (2000)
6. R. Mohan, M. Prasad Ghosh, R.K. Choubey, S. Mukherjee, J. Mater. Sci. Mater. Electron. **30**, 11748 (2019)
7. M.D. Stiles, R.D. McMichael, Phys. Rev. B **59**, 3722 (1999)
8. J. Nogués, J. Sort, V. Langlais, V. Skumryev, S. Suriñach, J.S. Muñoz, M.D. Baró, Phys. Rep. **422**, 65 (2005)
9. B. Dieny, V.S. Speriosu, S.S.P. Parkin, B.A. Gurney, D.R. Wilhoit, D. Mauri, Phys. Rev. B **43**, 1297 (1991)
10. B.A. Gurney, V.S. Speriosu, D.R. Wilhoit, H. Lefakis, R.E. Fontana Jr., D.E. Heim, M. Dovek, J. Appl. Phys. **81**, 3998 (1997)
11. J.R. Childress, R.E. Fontana, C. R. Phys. **6**, 997 (2005)
12. O.G. Heinonen, E.W. Singleton, B.W. Karr, Z. Gao, H.S. Cho, Y. Chen, IEEE Trans. Magn. **44**, 2465 (2008)
13. J.C.S. Kools, IEEE Trans. Magn. **32**, 3165 (1996)
14. S.S.P. Parkin et al., J. Appl. Phys. **85**, 5828 (1999)
15. S. Tehrani, B. Engel, J.M. Slaughter, E. Chen, M. De Herrera, M. Durlam, P. Naji, R. Whig, J. Janesky, J. Calder, IEEE Trans. Magn. **36**, 2752 (2000)
16. W.H. Meiklejohn, C.P. Bean, Phys. Rev. **102**, 1413 (1956)
17. V. Skumryev, S. Stoyanov, Y. Zhang, G. Hadjipanayis, D. Givord, J. Nogues, Nature (London) **423**, 850 (2003)
18. C.-H.T. Chang, S.C. Chang, J.S. Tsay, Y.D. Yao, Appl. Surf. Sci. **405**, 316 (2017)
19. M. Ali, P. Adie, C.H. Marrows, D. Greig, B.J. Hickey, R.L. Stamps, Nat. Mater. **6**, 70 (2007)
20. R. Pradheesh, H.S. Nair, V. Sankaranarayanan, K. Sethupathi, Appl. Phys. Lett. **101**, 142401 (2012)
21. S. Karmakar, S. Taran, E. Bose, B.K. Chaudhuri, C.P. Sun, C.L. Huang, H.D. Yang, Phys. Rev. B **77**, 144409 (2008)
22. E. Fertman, S. Dolya, V. Desnenko, L.A. Pozhar, M. Kajnakova, A. Feher, J. App. Phys. **115**, 203906 (2014)
23. R. Gupta, R. Ansari, A. Khandelwal, J. Fassbender, A. Gupta, Nuclear Instru. Methods B **266**, 1407 (2008)
24. R. Gupta, K.-H. Han, K.P. Lieb, G.A. Muller, P. Schaaf, K. Zhang, J. Appl. Phys. **97**, 073911 (2005)
25. R. Abrudan, J. Miguel, M. Bernien, C. Tieg, M. Piantek, J. Kirschner, W. Kuch, Phys. Rev. B **77**, 014411 (2008)
26. J.G. Ovejero, V. Godinho, B. Lacroix, M.A. García, A. Hernando, A. Fernández, Mater. Design **171**, 107691 (2019)
27. N.R. Panda, S.P. Pati, A. Das, D. Das, Appl. Surf. Sci. **449**, 654 (2018)
28. K. Simeonidis, C. Martinez Boubeta, O. Iglesias, A. Cabot, M. Angelakeris, S. Mourdikoudis, I. Tsiaoussis, A. Delimitis, C. Dendrinou Samara, O. Kalogirou, Phys. Rev. B **84**, 1 (2011)
29. M.A. Langell, M.D. Anderson, G.A. Carson, L. Peng, S. Smith, Phys. Rev. B **59**, 4791 (1999)
30. J.G. Cook, M.P. Van der Meer, Thin Solid Films **144**, 165 (1986)
31. E.A. Gulbransen, K.F. Andrew, J. Electrochem. Soc. **98**, 241 (1951)
32. Z.G. Wang, C. Dufour, E. Paumier, M. Toulemonde, J. Phys. Condens. Matter **6**, 6733 (1994)
33. K. Izui, S. Furuno, Proceedings of the 11th International Congress on Electron Microscopy, Kyoto 1986, edited by Timura, S. Maruse, and T Suzuki _Japan Society of Electron Microscopy, Tokyo, (1986), p 1299.
34. A. Meftah, F. Brisard, J.M. Costantini, M. Hage-Ali, J.P. Stoquert, F. Studer, M. Toulemonde, Phys. Rev. B **48**, 920 (1993)
35. F. Thibaudau, J. Cousty, E. Balanzat, S. Bouffard, Phys. Rev. Lett. **67**, 1582 (1991)
36. M. Toulemonde, Nucl. Instrum. Methods Phys. Res. B **156**, 1 (1999)
37. M. Toulemonde, C. Dufour, E. Paumier, Phys. Rev. B **46**, 14362 (1992)
38. J.A. Brinkman, J. Appl. Phys. **25**, 961 (1954)
39. J.A. Brinkman, Am. J. Phys. **24**, 246 (1956)
40. J.P. Biersack, L.G. Haggmark, Nucl. Instrum. Methods Phys. Res. **174**, 257 (1980)

41. T.J. Regan, H. Ohldag, C. Stamm, F. Nolting, J. Lunning, J. Stoehr, R.L. White, Phys. Rev. B **64**, 214422 (2001)
42. C.A.F. Vaz, E.L. Altman, V.E. Henrich, Phys. Rev. B **81**, 104428 (2010)
43. W.L. Roth, J. Phys. Chem. Solids **25**, 1 (1964)
44. A.K. Cheetham, D.A.O. Hope, Phys. Rev. B **27**, 6964 (1983)
45. M. Grimsditch, A. Hoffmann, P. Vavassori, H. Shi, D. Lederman, Phys. Rev. Lett. **90**, 257201 (2003)
46. X. Chen, C. Binek, A. Hoshstrat, W. Kleemann, Phys. Rev. B **65**, 012415 (2001)
47. C. Leighton, H. Suhl, M.J. Pechan, R. Compton, J. Nogues, I.K. Schuller, J. Appl. Phys. **92**, 1483 (2002)
48. H.-J. Kim, J.-H. Park, E. Vescovo, Phys. Rev. B **61**, 15284 (2000)
49. C.F. Chang, Z. Hu, S. Klein, X.H. Liu, R. Sutarto, A. Tanaka, J.C. Cezar, N.B. Brookes, H.-J. Lin, H.H. Hsieh, C.T. Chen, A.D. Rata, L.H. Tjeng, Phys. Rev. X **6**, 041011 (2016)
50. H.-J. Kim, J.-H. Park, E. Vescovo, Phys. Rev. B **67**, 15284 (2000)
51. J. Schlappa, C. Schußler-Langeheine, C.F. Chang, H. Ott, A. Tanaka, Z. Hu, M.W. Averkort, E. Schierle, E. Weschke, G. Kaindl, L.H. Tjeng, Phys. Rev. Lett. **100**, 026406 (2008)
52. E. Stavitski, F.M.F. de Groot, Micron **41**, 687 (2010)
53. D. Bazin, I. Kovacs, L. Guczi, P. Parent, C. Laffon, F. De Groot, O. Ducreux, J. Lync, J. Catalysis **189**, 456 (2000)
54. D. Su, S. Dou, G. Wang, Sci. Rep. **4**, 5767 (2014)
55. M. Shepit, V.K. Paidi, C.A. Roberts, J. van Lierop, Sci. Rep. **10**, 20990 (2020)
56. F.M.F. De Groot, M. Grioni, J.C. Fuggle, J. Ghijsen, G.A. Sawatzky, H. Petersen, Phys. Rev. B **40**, 5715 (1989)